High-field formation and field ion microscopy of monatomic carbon chains

2007 J. Phys.: Condens. Matter 19 466204

(http://iopscience.iop.org/0953-8984/19/46/466204)

IOP PUBLISHING JOURNAL OF PHYSICS: CONDENSED MATTER

J. Phys.: Condens. Matter **19** (2007) 466204 (10pp) doi:10.1088/0953-8984/19/46/466204

High-field formation and field ion microscopy of monatomic carbon chains

V A Ksenofontov, T I Mazilova, I M Mikhailovskij[1], E V Sadanov, O A Velicodnaja and A A Mazilov

National Scientific Center, Kharkov Institute of Physics and Technology, Academicheskaja, 1, 61108 Kharkov, Ukraine

E-mail: mikhailovskij@kipt.kharkov.ua

Received 14 June 2007, in final form 31 August 2007
Published 23 October 2007
Online at stacks.iop.org/JPhysCM/19/466204

Abstract

By methods of field ion microscopy and mass spectrometry, the presence of linear carbon chains at the surface of carbon fibers after high-voltage treatment using a pulse generator with pulse duration of 10 ns was revealed. The carbon chains attached to the specimen tips can be produced *in situ* in a field ion microscope using low-temperature pulsed evaporation by electric fields of the order of 80 V nm^{-1}. These nanowires are perfectly resolved in the field ion microscope. An analysis of the cluster images and determination of the field-enhancement factors strongly indicate that the field produced clusters are linear chains of one carbon atom in diameter. The process of field evaporation at the pulse voltage loading is sporadic with an anomalously large instant rate of evaporation corresponding to explosive removal of about 10^{11} atomic layers s^{-1}. Atomic C chains are produced during the high-field unraveling of nanofibers at 4.2 and 77 K.

1. Introduction

The field of quantum wires is moving at a rapid pace, with many potential applications in optics, sensors and electronics, to name a few. The research of linear carbon clusters C_n has recently exhibited striking growth due to its scientific importance and technological potential. Clusters C_n of various sizes have been registered in stellar atmospheres, in comet tails and in the interstellar space [1]. The continuing miniaturization of electronic devises raises the prospect of atomic wires with special mechanical and electrical properties [2–4]. This is mainly for the reason that linear atomic chains are viewed as having substantial potential as interconnects in nanoelectronics. Linear carbon clusters cannot, in general, be isolated in noticeable quantities and analyzed by traditional microscopic and spectroscopic means. As a consequence, just about

[1] Author to whom any correspondence should be addressed.

all the studies of structural and electronic properties of linear clusters have been carried out in molecular beams and in an inert matrix [2]. These studies showed that small carbon clusters are linear. For clusters with 7–10 atoms, linear and monocyclic rings are detected, whereas monocyclic structures are observed in between C_{11} and C_{20}. However, under the influence of an external electric field all these chains can be assumed to be linear.

In terms of recent laboratory studies of carbon clusters, mass spectrometry has been a most important means for the development of understanding of small carbon clusters. The production of carbon clusters can be realized by vaporizing a graphite target with an arc or an ion beam, or using the laser cluster beam technique. The high-temperature plasma produced condenses in carbon clusters whose morphology and charge state are controlled by quenching the plasma in an inert gas. The low-temperature mechanism of carbon cluster formation was realized by Ksenofontov *et al* [5] using a time-of-flight atom-probe. Charged carbon magic clusters of up to six atoms and 2^+ charges were found under pulse field evaporation of graphite fibers at cryogenic temperature. The magic carbon cluster ions produced by desorption under a high electric field were also observed in field-evaporation spectra of single-walled and multi-walled nanotubes in experiments by Hata *et al* [6]. The mechanism of non-activated selective formation of the magic cluster under the low-temperature and high-field conditions is not yet obvious.

Here, we report that linear carbon chains consisting of more than 10 atoms can be produced *in situ* in a field emission microscope using low-temperature pulsed-voltage field evaporation of needle-shaped carbon specimens. These chains are attached to the specimen tips and are perfectly resolved in the ion regime of the microscope.

2. Experimental details

Experiments were carried out in a two-chamber field ion microscope (FIM) in which the samples were cooled to 4.2 and 77 K [7]. Field images were formed by using helium gas under a pressure of 10^{-4}–10^{-3} Pa. The microscope was evacuated by cryogenic pumps to a residual gas pressure of about 10^{-7} Pa. Field ion and electron images were normally obtained in a voltage range 1–22 kV. Field-evaporation spectra of needle-shaped fibers were determined by using the mass-spectroscopic add-on device. Evaporation of ions subjected to mass analysis was implemented by a pulse generator with the front steepness of 20 ns and pulse duration of 10 ns at a level of 0.8 of the amplitude. The voltage pulse amplitude was varied from 0.5 to 7 kV. A total potential of 1–22 kV was applied between the specimen tip and the entrance aperture of a straight drift tube 1.50 m long. Field evaporation occurred under the action of the total voltage (a constant voltage required for the formation of the field ion image and a pulse voltage). The signals generated by individual ions or ionized clusters of atoms after the flight through the drift tube were detected by the chevron channel plate multiplier, and fed to the input of the timer.

Field-evaporation spectra in atom-probes are usually analyzed from the number of individual ion signals detected for different ion species. Since the time digitizer used with the chevron channel plate cannot discriminate signals according to the output pulse height, the ions with the same mass-to-charge ratio which arrive simultaneously at the detector are counted as only one signal. This problem is generally alleviated by operating the atom-probe at a very low counting rate. In this regime, the probability of pulse overlap becomes small, and the ion spectra derived should be accurate. But a preliminary study of the field evaporation of carbon specimens showed that this process is very irregular at low temperatures. A miscounting of simultaneously arriving ion signals cannot be eliminated even if the average evaporation rate of the carbon specimens is reduced below 0.01 atom/pulse. Usual time measuring devices were

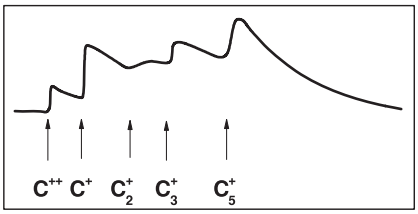

Figure 1. A time-of-flight mass-spectrum of cluster-wise field evaporation of the needle-shaped carbon nanofibers at 77 K.

not convenient in this case, and the flight times of the ions were measured with an oscilloscope. A high-voltage pulse removed the surface atoms in the form of singly or multiply charged ion clusters and activated a time sweep oscillator. The signal voltage increased proportionally to the number of ions (clusters) with the same mass-to-charge ratio, therefore the field-evaporation spectra could be derived from the signal intensities measured for various ion species.

Needle-shaped specimens having an initial radius of curvature at the tip in the range 20–50 nm and a length of about 3 mm were prepared from commercial carbon fibers by electrochemical etching in a 1 N KOH solution. The tip was fixed in the nickel tube with an outer diameter of 1.4 mm. The tip topography and microstructure were examined using a UEMB-100 transmission electron microscope (TEM). Carbon polyacrylonitrile-based fibers, which have a cross-sectional size of 7 μm and an average strength of 3.2 ± 0.8 GPa, are characterized by a homogeneous distribution of nanofibrils, the average size of which varies between 50 and 150 nm. The fiber structure is described by a random arrangement of flat or crumpled graphite sheets, with *a–b* planes running parallel to the fiber axis.

3. Results and discussion

3.1. Explosive field evaporation of carbon clusters

Several aspects in carbon cluster science can be investigated using low-temperature pulsed-voltage field evaporation. In pulse field evaporation of carbon, clusters produced are always charged and are accelerated at once in a high electric field, and so after the cluster is formed it no longer has any chance to interact with other clusters and atoms. Therefore, the abundance of cluster mass represents how carbon clusters are formed at the surface, the binding mechanism of clusters, and the absolute stability of the carbon species.

Under an averaged electric field of about 70–80 V nm^{-1}, carbon atoms are field evaporated mostly as C_n^+ clusters with $n = 2$–6. A typical scan illustrating the cluster-wise field evaporation of the needle-shaped carbon nanofiber is shown in figure 1. This time-of-flight mass spectrum is obtained at a low level of the signal voltage amplification, which precludes the possibility to detect single ions. The height of steps at the oscillogram is proportional to the number of clusters with the same mass-to-charge ratio. Taking this fact into account, we showed that the maximum number of carbon atoms registered by the detector is about 10^3 atoms/pulse at the average evaporation rate of the carbon specimens of about 1 atom/pulse. Consequently, these results confirm our preliminary conclusion about significant irregularity of the field evaporation process for carbon specimens at low temperatures. The process of field evaporation at the pulse voltage loading is sporadic with an anomalously large instant rate of evaporation corresponding to explosive removal of about 10^{11} atomic layers s^{-1}. This process was controlled by using the TEM with the resolution of 0.4 nm. It was shown that explosive

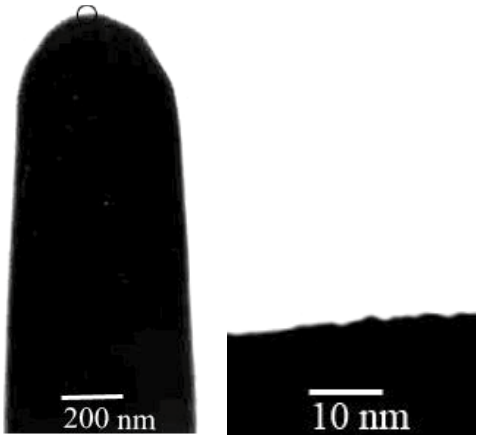

Figure 2. Electron microscope low- (a) and high-magnification (b) images of the pointed carbon fiber after low-temperature field forming at 5.80 kV.

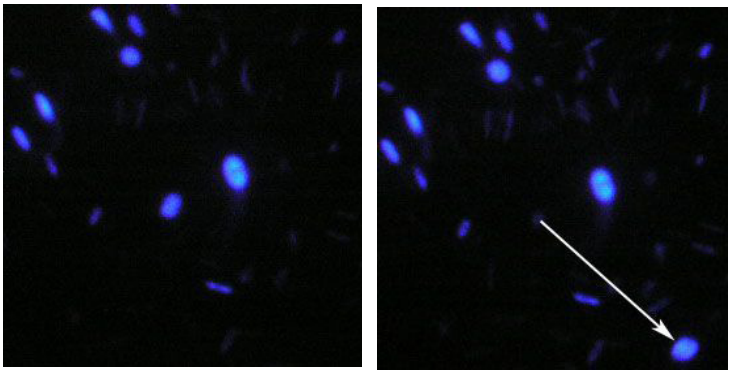

Figure 3. FIM micrographs of the pointed carbon fiber after low-temperature field forming acquired at 4.20 (a) and 4.35 kV (b).

(This figure is in colour only in the electronic version)

field evaporation is accompanied by significant blunting and smoothing of the needle-shaped carbon specimens (figure 2).

3.2. The field-enhancement factor for the carbon atomic chains and nanoprotrusions

Figure 2 shows the TEM images of the carbon tip acquired after surface forming by field evaporation at 4.2 K and FIM studies. Figure 2(a) displays a representative overview micrograph of the high-field formed carbon tip. The specimen having initial radius of curvature r_0 about of 35 nm was blunted during a steep ($\sim$5 V s^{-1}) increase of voltage V up to 5.80 kV to $r_0 = 250$ nm. Figure 2(b) shows a higher-magnification image of the region outlined by a circle in figure 2(a) and reveals nanoscale undulations formed during field evaporation. The average height L and radius of curvature ρ of nanoprotrusions are 1.5 and 5.0 nm, correspondingly.

Figure 3 shows the FIM images of the carbon tip after surface forming by field evaporation at 4.2 K. FIM images consist of randomly distributed bright spots. During a field increase, the

brightness of the image spots enhances. The FIM images shown in figures 3(a) and (b) illustrate the frequently observed process of long-range jumps of image spots at some stage in the voltage increase. The arrow in figure 3(b) shows the direction and length (about 23 nm) of the individual image spot jump during the voltage V increase from 4.20 to 4.35 kV. The main attribute of the FIM for the investigation of an atomic topography is its ability to reveal the location of atomic protrusions on a surface formed by field evaporation. Such protrusions are characterized by an enhancement in the local electric field. Due to the nature of the image formation process, these local field enhancements produce high-contrast image spots on a uniformly dark background. The observation of long jumps of bright FIM image spots during a high-field treatment shown in figure 3 points out that in this case a local field enhancement at bright image spots is not due to a very sharp microprotrusion on the graphite tips.

The field-enhancement factor can be defined as

$$\beta = F/F_M, \tag{1}$$

where F is a local field and F_M is the macroscopic field defined as $F_M = V/D$. Here D is the interelectrode distance in a geometrical configuration resembling a parallel-plate capacitor. In our experiments a voltage corresponding to the threshold of low-temperature field evaporation ranging from 2.5 to 22 kV was applied on the electrodes with D of about 5 mm. As was shown above, low-temperature field evaporation of carbon takes place at electric field strength F of about 70–80 V nm^{-1}. Consequently, one can obtain the calculated value of the field-enhancement factor in the range of $1.59 \times 10^4 < \beta < 1.33 \times 10^5$. The extremely large field-enhancement factors have been reported previously from field electron emission measurements made over large areas and individual tips [8–10]. Huang *et al* showed that a giant field-enhancement factor (up to 1.88×10^4) is a result of a multistage structure of the nanoemitters [9]. Their structure is characterized by an order of magnitude smaller features (nanotubes or nanowires), growing at the tips of larger features. A multistage structure, with each stage much smaller than the previous one, is characterized by the total field-enhancement factor at the tip of the smallest feature given by

$$\beta_{\text{tot}} = \prod_{i=1}^{m} \beta_i, \tag{2}$$

where m is the total number of stages, i is the stage index. The experimental value of the total field-enhancement factor for the specimen shown in figure 2 formed by evaporation at electric field $F_{\text{ev}} = 75 \pm 4$ V nm^{-1} can be found from

$$\beta_{\text{tot}} = \frac{F_{\text{ev}} D}{V}. \tag{3}$$

By using the value of D equal to 5 ± 0.5 mm, we obtain the experimental value $\beta_{\text{tot}} = 6.47 \times 10^4$.

The value of β_1 corresponds to the mesoscopic field-enhancement factor at the apex of carbon needle-shaped emitters. The electric field and potential distribution between such a tip and a counter-electrode can be considered in terms of the hyperboloidal model [11]. In this approximation, the tip and counter-electrode are represented by two confocal hyperboloids of revolution. A local field F at the tip surface is a logarithmic function of the radius of curvature and D. Taking r_0 to be the radius of curvature at the specimen apex, simple transforms of the equation for F yielded the following expression for the mesoscopic field-enhancement factor in the hyperboloidal approximation:

$$\beta_1 = \frac{2D}{r_0 \ln(\frac{4D}{r_0})}. \tag{4}$$

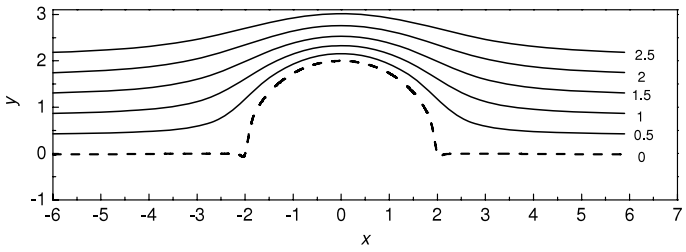

Figure 4. Equipotential lines generated by the hemisphere on a plane. The numbers near the equipotentials denote the potential in volts.

Thus, from equation (4) for the specimen shown in figure 2, the mesoscopic field-enhancement factor is equal to 3.54×10^3 and $\beta_1 \ll \beta_{\text{tot}}$. Such a discrepancy shows that the carbon specimen formed by field evaporation has a multistage structure and the local electric field is determined to a considerable degree by smaller topographic features.

A certain contribution to β_{tot} is introduced by an additional enhancement of the local field in the vicinity of the nanoscale undulations shown in figure 2(b). But it is intuitively clear that observed nanoprotrusions with low aspect ratios cannot be responsible for a high discrepancy of the experimental and theoretical field-enhancement factors. To our knowledge the field-enhancement factors were calculated only for protrusions with high ratios of the total protrusion length to the base radius ($\nu = L/\rho \geqslant 1$) [8, 9, 12]. In this range of the ratio ν two analytical models give satisfactory results: the 'hemisphere on the plane' model and the 'hemisphere on a post' model ([12] and references therein).

In terms of the hemisphere on the plane model the potential at the sphere surface is given by a superposition of the field of a dipole of strength $p = 4\pi\varepsilon_0\rho^3 F_M$ located at the center of a hemisphere of radius ρ and a planar charge sheet of density $\varepsilon_0 F_M$, where ε_0 is the electric constant:

$$\varphi = -\frac{p\cos\theta}{4\pi\varepsilon_0 r^2} + r F_M \cos\theta. \tag{5}$$

Here (r, θ) denote the spherical coordinates with the origin in the sphere center. The total potential at any point on the hemisphere surface is zero: the emitter plane and the hemisphere boss surface constitute an equipotential with $\varphi = 0$. Figure 4 shows the calculated potential distribution in the vicinity of the hemisphere on a plane. The equipotential lines are bent around the hemisphere producing an enhancement of the applied electric field. These data can be used for a determination of the field-enhancement factor for smooth protrusions with $\nu < 1$. To pursue this object, we calculated a family of equipotentials such that one coincides with the protrusion surface and one with the counter-electrode. Such a representation for rather short nanoprotrusions was given in Cartesian coordinates (x, y).

It was found that the geometry of a typical nanoprotrusion could be fitted accurately by one equipotential surface from the set surrounding a charged body which consisted of an isolated hemisphere on the plane. Figure 5 illustrates this possibility for an approximation of one rather short nanoprotrusion on the specimen with $\nu = 0.24$ shown in figure 2. The surface of the nanoprotrusion coincides with an equipotential surface of value $\varphi\,(x, y) = 2$ V.

Figure 6 (curve 1) gives the nanoscopic field-enhancement factor β_2 obtained from equation (5) as a function of aspect ratio for $\nu < 1$. For $\nu < 1$, the values of ρ were determined at the apex of the matching equipotentials. The field enhancement was obtained from equation (5) using the gradient of φ at the apex equipotentials. It demonstrates the well known exact result that the local field-enhancement factor at the hemisphere apex ($\nu \to 1$) is

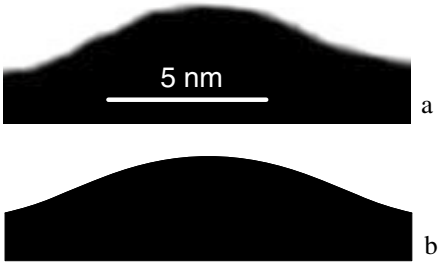

Figure 5. Electron microscope image (a) of the nanoprotrusion on the carbon tip formed by field evaporation and its electrostatic approximation (b). For the matching equipotential $\varphi\ (x, y) = 2$ V.

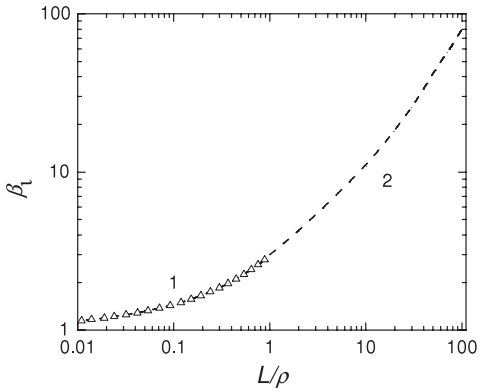

Figure 6. The field-enhancement factor as a function of the aspect ratio $\nu < 1$ (curve 1). The dotted line 2 corresponds to equation (7) for $\nu > 1$.

three. In the range $0.01 \leqslant \nu \leqslant 1$ the factor is represented, to within 4%, by

$$\beta_2 = 1.19 + 2.30\nu - 0.49\nu^2. \tag{6}$$

In the vicinity of $\nu = 1$ our results are very close to that for $\nu > 1$ (curve 2 in figure 6) represented by the approximation [12]

$$\beta_P = 1.2\,(\nu + 2.15)^{0.90}, \tag{7}$$

obtained for the 'hemisphere on a post' model.

For the average value of the aspect ratio $\nu = 0.30$ for nanoprotrusions on the specimen under consideration equation (6) gives the field-enhancement factor β_2 of 1.84 and $\beta_1\beta_2 = 6.51 \times 10^3$. The magnitude $\beta_1\beta_2$ is much smaller than the experimental total field-enhancement factor ($\beta_{\text{tot}} = 6.47 \times 10^4$). To interpret this result, we can conclude that the carbon emitters with nanoprotrusions formed by field evaporation are not atomically smooth electrodes but have atomic-scale features possessing high aspect ratios, invisible in TEM. An atomic-scale β_3 is equal to $\beta_{\text{tot}}/\beta_1\beta_2$. The specimen shown in figure 2 has the atomic-scale field-enhancement factor $\beta_3 = 9.94$. This value corresponds to atomic-scale protrusions at the apex of nanoprotrusions. For flat parts of the needle-shaped carbon specimen $\beta_2 \approx 1$, and therefore $\beta_3 = 15.3$. The most available candidate for such a high field-enhancement factor β_3 is the normal to surface atomic carbon wires with a rather high aspect ratio.

To determine the length of C nanowire on the needle-shaped electrode we used the model [13], in which the nanowire stands normally, having length L and radius $\rho = 1.2$ Å.

Taking into account that $\rho \ll r_0$ the mesoscopic electrode (hyperboloid) can be replaced by a plane. In this case equation (7) is valid and gives the aspect ratios of 8.34 and 14.79 and the lengths of the nanowires of $L = 11.9$ and 18.4 Å for $\beta_3 = 9.94$ and 15.3, accordingly. The bond length structures of C-wires are essentially cumulenic with only a small dimerization with bond lengths between 1.27 and 1.29 Å [2]. So for appraisal the use of a constant interatomic distance $d = 1.28$ Å is satisfactorily accurate. The numbers of carbon atoms in a linear chain estimated as $n \approx L/d + 1$ were equal to 10 and 15 for these two field-enhancement factors on the surface of a typical carbon tip.

3.3. Unraveling of graphene sheets

As was shown by Smalley and collaborators, monatomic chains can be formed by the unraveling suggested in field electron emission experiments with carbon nanotubes, where the electric force unravels the multi-walled tube like the sleeve of a sweater [14], and by mechanical pulling of carbon nanotubes [15]. To examine the mechanism and trend for atomic chain formation in high electric fields, we carried out detailed calculations of the graphene unraveling. The numerical simulations were carried out using the classical molecular dynamics method, employing the short-range Tersoff–Brenner bond order potential [16], which reproduces lattice constants, binding energies, and the mechanical properties of diamond, graphite, and carbon nanotubes.

The electric force producing an axial tension is localized at the top of the chain. In our molecular dynamics modeling the electric force was 4.0–5.4 nN. Figure 7 shows a linear carbon chain extending out from the graphene layer under the action of electric field at the beginning (a) and after 3.2×10^{-14} s (b), 6.4×10^{-14} s (c) and 9.6×10^{-14} s (d). The nanowire is held taut in this case by the electric force of 5.3 nN.

At first, the dangling bond {0}–{1} at the graphene edge orients along the electric force (figures 7(a) and (b)). After this the weakest link has proved to be the nearest bond {1}–{2} aligned along the applied electric force. This bond stretches and finally breaks up first under a local force produced by a high electric field (figure 7(b)). After this the atomic wire becomes longer and straightens under the action of an electric field. The resulting effect is to increase the chain length by two atoms without any change in bond order of the open edge of the graphene sheet. The atomic chain extending out from the graphene edge is held straight and taut by the electric field (figure 7(b)). Further pulling of the atomic chain by the electric field repeats the described sequence of events, unraveling the linear carbon. The second bond normal to the surface of the graphene sheet also starts to stretch and breaks up (figure 7(c)). In figure 7(d) one can observe an eight-atom chain that detached from the graphene edge. Therefore, the disintegration process is successive and clearly localized, with a sudden complete drop in the local failure force due to the bond breaking.

The orientation of electric force favors breaking the {1}–{2} and {4}–{5} bonds normal to the open edge of the graphene layer. It is also essential that the failure force of the linear carbon chain is slightly higher than those of the graphene bonds. The energy per bond in general depends in a complicated way on the geometry. However, as was shown by Abel [17] and Tersoff [18], for covalently bonded systems the most important variable appears to be the coordination number. The bond strength of carbon atoms is a monotonically decreasing function of the number of nearest-neighbor atoms close enough to form bonds. If the bond energy decreases rapidly with the coordination number, then the linear atomic chains along with the diatomic molecule will be characterized by a high value of the bond strength. This effect for carbon interatomic bonds quantitatively described by the Brenner version [16] of the Abel–Tersoff bond order formalism used in our simulation.

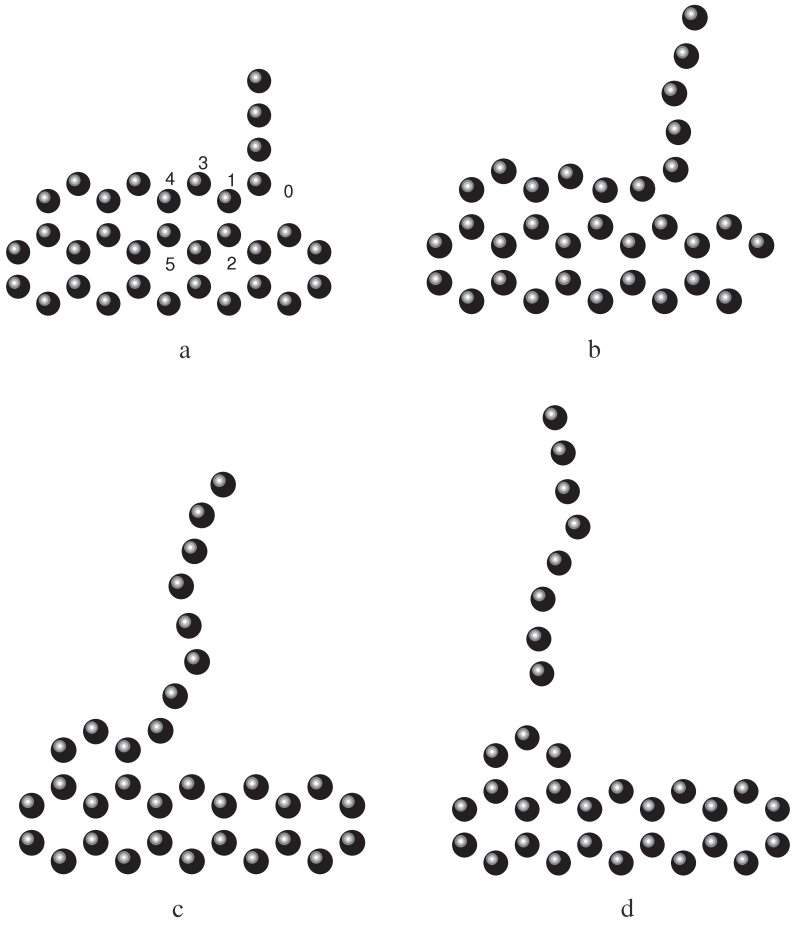

Figure 7. Forming of the carbon nanowire during the unraveling of a graphene sheet. Labels (a)–(d) denote the various unraveling stages.

The high-contrast image spots in figure 3 correspond to apexes of atomic wires on the carbon tip produced during the high-field unraveling. Experimentally observed translation motion of the image spots along the surface far beyond atomic dimensions may be considered as a long-range unraveling along the graphene edges. We can suppose that ions are evaporated from a carbon surface initially in linear cluster forms, which decompose mostly into smaller atomic clusters and individual ions because of thermal excitation during unraveling and Coulomb explosion.

4. Conclusions

To summarize, we present the field ion microscopic and mass-spectroscopic evidence of the presence of linear carbon chains at the surface of carbon fibers after high-voltage treatment using a nanosecond pulse generator. The linear carbon chains attached to the needle-shaped specimen can be produced using low-temperature field evaporation. The apexes of these chains are entirely resolved in the field ion microscope. The determination of the field-enhancement factors and analysis of the cluster images indicate that the field produced clusters are linear

chains with a high aspect ratio. The atomic carbon chains can be produced during the high-field unraveling of graphenes at low temperatures. The process of low-temperature field evaporation at the pulse voltage loading is sporadic with an explosive instant rate of removal of surface atoms.

Acknowledgments

This work was supported by the NATO International Program No. SA (PST.CLG.976376) 5437 and the Deutsche Forschungsgemeinschaft (DFG grant 436 UKR 17/26/06).

References

[1] Terzieva R and Herbst E 2000 *Int. J. Mass. Spectrosc.* **201** 135
[2] Bianchetti M, Bounsante P F, Ginnelli F, Roman H E, Broglia R A and Alasia F 2002 *Phys. Rep.* **357** 459
[3] Riberto F J, Roundy D J and Cohen M L 2002 *Phys. Rev.* B **65** 153401
[4] Lang N D and Avouris P 2003 *Nano Lett.* **3** 737
[5] Ksenofontov V A, Kulko V B and Mikhailovskij I M 1983 *Sov. Phys.—Tech. Phys.* **28** 973
[6] Hata K, Ariff M, Tohji K and Saito Y 1999 *Chem. Phys. Lett.* **308** 343
[7] Mikhailovskij I M, Smith G, Wanderka N and Mazilova T I 2003 *Ultramicroscopy* **95** 157
[8] Umnov A G, Shiratori Y and Hiraoka H 2003 *Appl. Phys.* A **77** 159
[9] Huang J Y, Kempa K, Jo S H, Chen S and Ren Z F 2005 *Appl. Phys. Lett.* **87** 053110
[10] Chen H J H and Hung C S 2007 *Nanotechnology* **18** 355305
[11] Miller M K, Cerezo A, Heatherington M G and Smith G D W 1996 *Atom Probe Field Ion Microscopy* (Oxford: Clarendon)
[12] Forbes R G, Edgcombe C J and Valdre U 2003 *Ultramicroscopy* **95** 57
[13] Lorenzoni A, Roman H E, Alasia F and Broglia R A 1997 *Chem. Phys. Lett.* **276** 237
[14] Rinzler A G, Hafner J H, Nikolaev P, Lou L, Kim S G, Tomanek D, Norlander P, Colbert D T and Smalley R E 1995 *Science* **269** 1550
[15] Marques M A, Troiani H E, Miki-Yoshida M, Jose-Yacaman M and Rubio A 2004 *Nano Lett.* **4** 811
[16] Brenner D W 1990 *Phys. Rev.* B **42** 9458
[17] Abel G C 1985 *Phys. Rev.* B **31** 6184
[18] Tersoff J 1988 *Phys. Rev. Lett.* **61** 2879